ICAS 2020 SHANG HAI
International Council of the Aeronautical Sciences
32nd Congress of the International Council of the Aeronautical Sciences
September 6-10, 2021
Pudong Shangri-La, Shanghai, China

Effect of Inter-stage Bleeding on Flow Stability of a Multi-stage Compressor

Xiwu LIU[1], Hailiang JIN[1], Daobin QIU[1] & Yueqian YIN[1]

[1] AECC Hunan Aviation Powerplant Research Institute, Hunan Key Laboratory of Turbomachinery on Small and Medium Aero-Engine, ZhuZhou, China, 412000

Abstract

The effect of inter-stage bleeding on flow stability of a multi-stage compressor was investigated through computational fluid dynamics (CFD) method. The bleed air is taken out at the outlet of the 2nd stage through a circumferential slot to an annular chamber, and then the bleed air is released through two axisymmetric off-take ducts. The calculation results show that the surge margin as well as the matching of the multi-stage axial compressor at part speed has been improved by bleeding. There is an optimal bleed flow rate in order to get a wider operating range and higher peak efficiency (PE) under a specific corrected rotational speed. The optimal bleed flow rate increase when the corrected rotational speeds decrease. The flow mechanism of the inter-stage bleeding is the reduction of the large positive incidence angle of the first stator (S1), as well as the alleviation of the blockage of the back-stages. The mismatching of the different stages has been relieved.

Keywords: compressor, bleeding, flow stability, CFD, matching

1. Introduction

The design point or matching point of a compressor is usually chosen where the compressor will operate for the most of the time or where the performance is particularly critical. This working condition is generally near the maximum pressure rise or peak efficiency of the compressor [1]. For the gas turbine engine, the machine must deliver enough pressure rise and efficiency, at the same time it must also provide sufficient surge margin at part speed, especially at the startup of the engine.

At design point or matching point the incidence angle of the blade rows of the multi-stage compressor is generally near their optimal incidence. When the compressor is work at the off-design conditions, i. e. near choke or near stall at the same corrected speed or on the working line at different corrected speed, the stages matching of the multi-stage compressor will change, and the mismatching will occur. At this condition, the incidence of each blade rows cannot work at their optimal. At low part speed, the mass flow rate is at low level, the incidence angle of the front stages increase, and the operating point will move to the near stall point. For the rear stages, the annulus convergence flow path is design for the design speed. However, the pressure rise and density are lower than the design values at part speed. Thus the axial velocity at part speed will be higher than the design speed, and the incidence angle of the rear stages decrease, this will lead to the rear stages work at near choke condition [2]. In order to solve this problem, the techniques of inter-stage bleed or variable stagger stator are commonly used in the gas turbine engine to correct the incidence angle of the stages. Several arrangements of slots and bleed holes have been investigated by Leishman et al. [3] [4]. Conan et al. [5] and Wellborn et al. [6] conducted a numerical investigation of the uniform bleed on the internal flow stability of the compressor. A non-uniform bleed on the internal flow stability of the compressor through annulus cascade was conducted by Gomes et al. [7] [8]. The shape or arrangements of the bleed slots, annulus chamber, and off-take ducts all can be customized. The results of the Gomes et al. studies show that the non-uniform bleed will introduce total pressure distortion at circumferential direction. This may lead to the deterioration on the stability of the compressor. However, there are no other stages at the

outlet of their annulus cascade; no further explanation is given by Gomes et al.

Through the literature review the authors find that there is little investigation on the numerical calculations on the effects of real bleed slots, bleed chamber and off-take ducts. In this paper, steady state numerical calculations have been conducted in order to get a better understanding of the effects of real bleed system structure on the internal flow stability of a multi-stage compressor.

2. Multi-Stage Axial Compressor

The numerical calculations described in this paper were performed in a 4 stages low pressure compressor as shown in Fig. 1. Bleed air is extracted from the compressor through a bleed system, which consists of a circumferential bleed slot, an annular plenum chamber, and double axisymmetric off-take ducts. The bleed system is shown in Fig. 2. The circumferential bleed slot is located at the downstream of the 2nd stage stator casing, which is also located at the upstream of the 3rd stage rotor casing. Either of the double axisymmetric off-take ducts can be shutdown, based on the mass flow of the bleed air. When both of the off-take ducts were shutdown, this condition was regarded as the datum (without bleed).

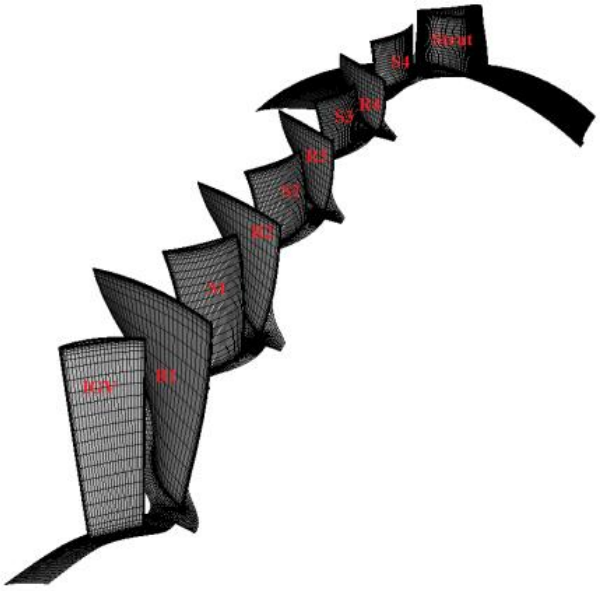

Figure 1 –Multi-Stage Axial Compressor.

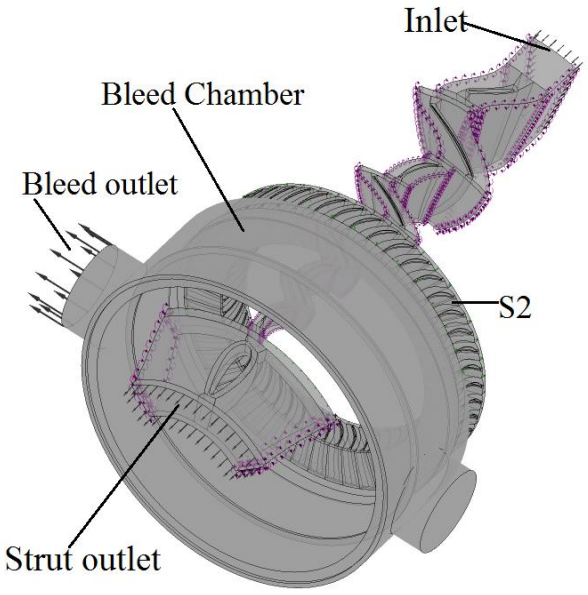

Figure 2 –Multi-Stage Axial Compressor with inter-stage bleed.

3. Numerical Approach

The numerical calculations were performed by adopting the CFD package of ANSYS CFX.

The computational meshes of the multi-stage axial compressor were generated with grid generation tool of NUMECA/IGG, the meshes were shown in Fig. 3. The total number of nodes was chosen to be about 7 million. The structured mesh of the bleed system was generated with grid generation tool of ICEM. The mesh of the off-take ducts adopted in this paper is butterfly mesh.

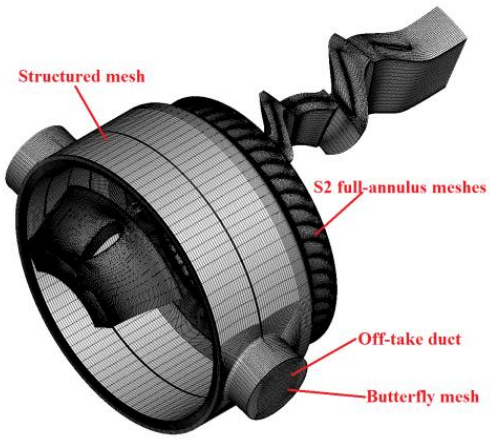

Figure 3 –Meshes of the multi-stage axial compressor.

K-epsilon turbulence model was adopted in the CFD calculation. The y+ on the blade and endwall was controlled within 50, in order to meet the requirement of the turbulence model.

The average static pressure condition was specified at the strut outlet, mass flow rate was specified at the outlet of the bleed off-take duct (when only one of the two off-take ducts was used, the bleed off-take duct boundary type was set as outlet, the other off-take duct boundary type switch to wall condition). Total pressure and total temperature at standard day (101325Pa, 288.15K) was specified at the inlet boundary. The mixing-plane model was adopted at the rotor/stator interface. The solid surfaces were prescribed with adiabatic boundaries.

During the numerical calculation, the specific corrected speed line can be obtained through increasing the back pressure at the strut outlet. When the global residuals reach the convergence criteria, and the fluctuation in the inlet/outlet mass flow rate, pressure ratio, and adiabatic efficiency become stabilized, then the calculation results were considered as convergence results. The last convergence result before divergence was considered as the stall point (not the real stall) as the back pressure increasing.

The inlet guide vane (IGV) and the first stator (S1) were designed as variable, but only the IGV was used during the part speed calculation. The control law of the IGV and S1 at different corrected speed is shown in Fig. 4. In Fig. 4 the '*Rot_angle*' in the ordinates stands for IGV or S1 variable stator stagger adjust angle, subscript '*ref*' in the ordinates stands for reference location which is the variable stator stagger adjust angle at 60% corrected speed, N_c in the coordinates stands for the corrected rotational speed.

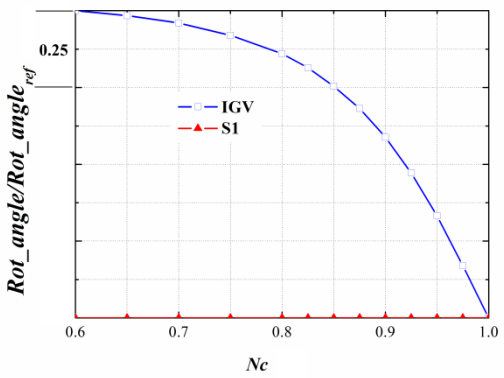

Figure 4 –IGV and S1 control law at different corrected rotational speed.

4. Results and Discussion

4.1 The Pressure Ratio and Efficiency Characteristics

The pressure ratio and efficiency characteristics of the multi-stage axial compressor with and without bleeding are shown in Fig. 5 and Fig. 6. The cancelling of dimensions of pressure rise, efficiency, and the corrected speed has been used in the presentation of the pressure ratio and efficiency characteristics of the multi-stage axial compressor. The cancelling of dimensions is achieved by choosing a reference point on the pressure ratio and efficiency characteristics. In this paper, the reference point was chosen to be the peak efficiency point at 80% corrected speed without bleeding.

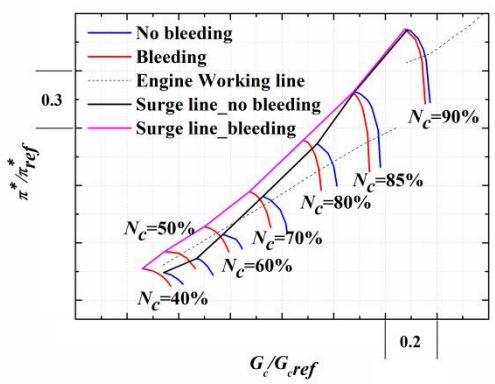

Figure 5 –Pressure ratio characteristic of the multi-stage axial compressor with and without bleeding.

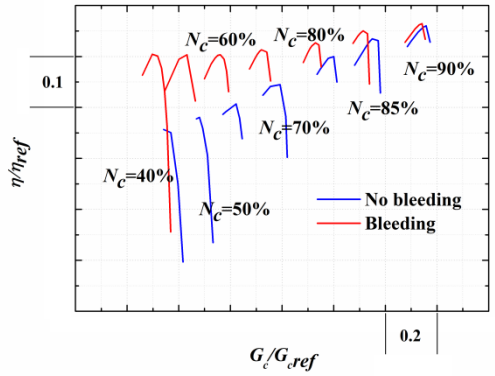

Figure 6 –Efficiency characteristic of the multi-stage axial compressor with and without bleeding.

It can be seen from Fig. 5 that the change of the surge margin of the multi-stage axial compressor at 85% and 90% corrected speed is negligible. The main change at 85% and 90% corrected speed is the adiabatic efficiency as shown in Fig. 6. Through bleeding the mismatching of the stages relieved, i.e. the operating point gets a better matching. This is main reason that the adiabatic efficiency increase by bleeding off some air from the middle stages. For other part speed (N_c vary from 40% to 80%), the surge line move to the top left side of the pressure rise-mass flow characteristic. This means the surge margin has been increased significantly. Especially, when the corrected speed is lower than 70%, without bleed the working line is at left side of the surge line, by bleeding off some air the working line moves back to the right side of the surge line. The increasing of the surge margin is also related to the relief of the mismatching of the stages. It should be noted that the calculation of the efficiency with bleeding did not consider the losses introduced by the bleed; this is the main reason that the efficiency has significant difference with and without bleeding. The main considerations for adopting this efficiency calculation method is that the major function of the bleed is to improve the surge margin, in addition, the bleed operating time is short and is only used to pass the low and middle corrected speed, thus there is no need to calculate of the real efficiency with bleeding.

4.2 Optimal Bleed Mass Flow Rate

The bleed mass flow rate at different corrected rotational speed in Fig. 5 and Fig. 6 is the optimal bleed mass flow at corresponding corrected speed. A brief description of the method to get the optimal bleed mass flow at 80% corrected speed will be given in the following passage. Constant mass flow rate bleed is adopted in this paper at a specific corrected rotational speed. The trends of surge margin and efficiency along with the bleed mass flow rate are shown in Fig. 7 and Fig. 8. There are many different ways of defining surge margin, two of the most commonly used definitions are adopted in this paper. One of the simplest definitions is defined in Eq. (1).

$$SM_{pr} = \frac{(PR_s - PR_W)}{PR_W} \times 100\% \tag{1}$$

Where *PR* denotes pressure ratio, subscript '*S*' and '*W*' denote the operating point at surge and working point respectively.

The other commonly used definition of the surge margin as defined by Cumpsty [1] is given by Eq. (2).

$$SM = 1 - \left(\frac{PR_W}{PR_S} \times \frac{G_{c:S}}{G_{c:W}} \right) \times 100\% \tag{2}$$

Where $G_{c:S}$ and $G_{c:W}$ denote corrected mass flow rate at surge and working operating point respectively.

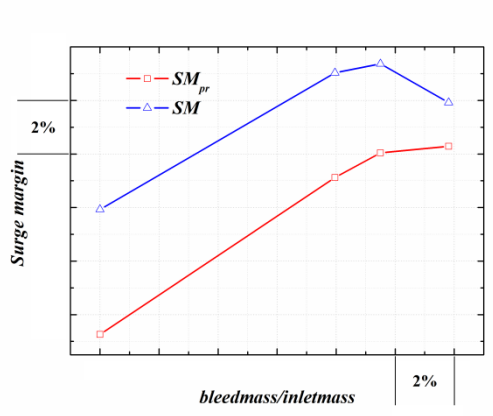

Figure 7 –Trends of the surge margin along with the bleed mass flow rate.

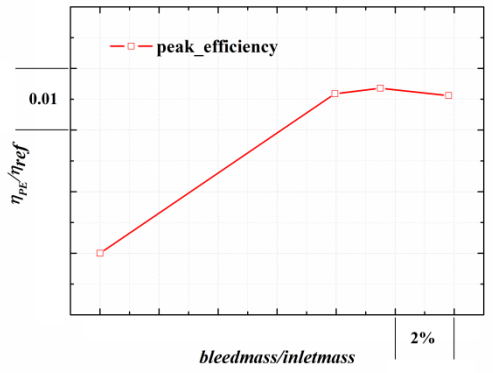

Figure 8 –Trend of the efficiency along with the bleed mass flow rate.

At 0% mass flow rate, i. e. without bleeding, the surge margin SM_{pr} and *SM* is low, as the bleed mass flow rate increase, the surge margin SM_{pr} and *SM* also increase. When the bleed mass flow reaches about 10% inlet mass flow, the *SM* reaches its maximum value. The variation of *SM* along the bleed mass flow rate is thought to be caused by the changing of the stages matching, at lower bleed flow rate, the mismatching of the stages cannot be relieved. This is also consistent with the change of the incidence angle with the mass flow. At part speed, the front stages tend to operate near the stall point, while the rear stages tend to operate near the choke point. As the bleed mass

flow increase, the incidence of the front stages will be reduced, the operating point of the front stage will move to its optimum incidence, the surge margin increase. As the bleed mass flow continues to increase, the incidence will decrease to a negative incidence, and the operating point will move to the choking point, the surge margin will decrease. Therefore, there is an optimal bleed mass flow in order to get maximum surge margin. It can be seen from Fig. 7 that the maximum value of the SM_{pr} and SM do not have the same bleed mass flow rate, in order to decide which surge margin is the better one, the peak efficiency along the bleed mass is illustrated in Fig. 8. It can be seen that the bleed mass flow is also about 10% when the efficiency reaches its maximum, this bleed mass flow is consistent with the optimal mass flow of the SM. Therefore, the surge margin definition SM is chosen as the suitable definition. The optimal bleed mass flow rate at different corrected rotational speed is shown in Fig. 9. It can be seen that the lower the corrected speed; the greater the amount of bleed mass flow is needed to be extracted from the middle stage.

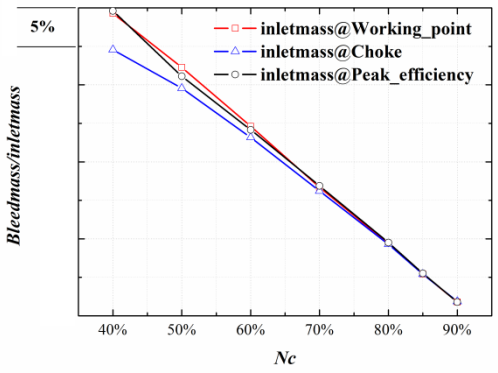

Figure 9 –Optimal bleed mass flow rate at different corrected rotational speed.

4.3 Stage Characteristic and Flow-Field Analysis

In order to get a clearer picture of the variation of the operating point at part speed, the stage loading-flow coefficient characteristic of the compressor at 80% corrected speed is given in Fig. 10. The flow coefficient is defined in Eq. (3).

$$\phi = \frac{V_x}{U_{tip}} \tag{3}$$

Where V_x denotes the axial velocity and U_{tip} is the blade tip speed.

The stage loading is defined in Eq. (4).

$$\psi = \frac{\Delta h}{U_{tip}^2} \tag{3}$$

Where Δh denotes the enthalpy change, and U_{tip} is the blade tip speed.

It can be seen that without bleeding the front stages (1st and 2nd stage) have the tendency to move towards stall; and the rear stages (3rd and 4th stage) have the tendency to move to the choke or negative incidence stall, and the compressor becomes mismatched. With some air extracted from the middle stage, the front stages move away from the stall, and the rear stages move away from choke, and the compressor moves back to the matching point.

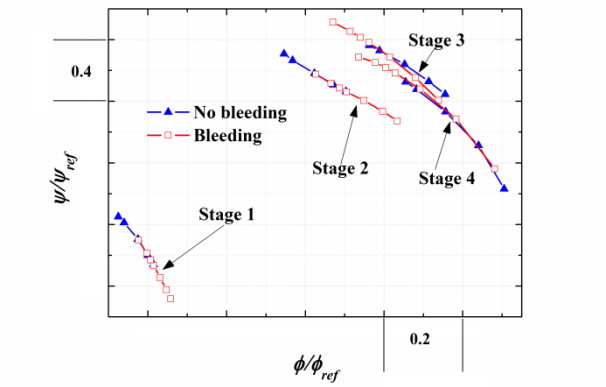

Figure 10 –Stage loading-flow coefficient characteristic of the compressor at 80% corrected rotational speed.

The contours of relative Mach number on the blade-to-blade surface on 50% span with the optimal bleed mass flow rate and without bleeding at 80% corrected speed peak efficiency point are shown in Fig. 11 and Fig. 12. It can be seen that without bleeding there is a major separation on the suction surface of S1 (as shown in Fig. 11). With the optimal bleed mass flow rate, the suction surface separation of the S1 has been suppressed (as shown in Fig. 12). This is caused by the reduction of the incidence angle of the S1 by bleeding of some air from the middle stage.

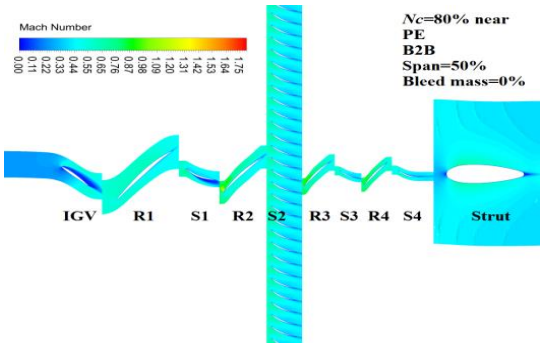

Figure 11 –Contour of relative Mach number on the blade-to-blade surface on 50% span without bleed at 80% corrected speed peak efficiency point.

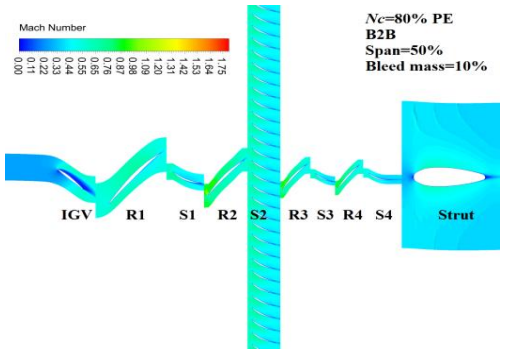

Figure 12 –Contour of relative Mach number on the blade-to-blade surface on 50% span with optimal bleed mass flow rate at 80% corrected speed peak efficiency point.

From Fig. 11 and Fig. 12 it can be seen the major Mach number difference is on the S1 with and without bleeding. In order to get a clearer understanding of the flow structure of S1, the surface streamline on the suction surface of S1 with the optimal bleed mass flow rate and without bleeding at 80% corrected speed peak efficiency point is illustrated in Fig. 13. Without bleeding, there is large flow separation on suction surface across the full span of the S1. Especially two focus points which are located at about 40% and 70% span-wise location respectively. When about 10% of the inlet mass flow is extracted from the main flow, the flow separation especially two of the focus points on the suction surface disappear. This is thought to be caused by the reduction of the incidence angle of S1. In order to confirm the incidence reduction, the contour of Mach number on

the blade-to-blade surface on different span-wise locations with the optimal bleed mass flow rate and without bleeding at 80% corrected speed peak efficiency point are given in Fig. 14-Fig. 16.

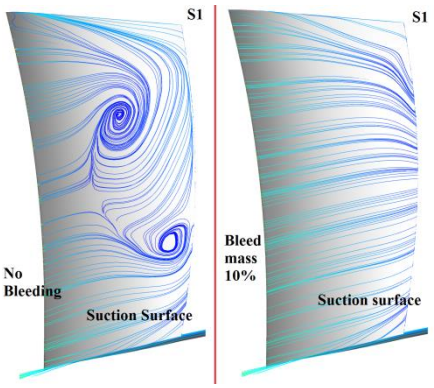

Figure 13 –Surface streamline on the suction surface of S1 with the optimal bleed mass flow rate and without bleeding at 80% corrected speed peak efficiency point.

It can be seen from Fig. 14-Fig. 16 that the flow separation on the suction surface without bleeding has been suppressed. As mentioned before, the main reason for this is thought to be the reduction of incidence angle after bleed off some air. The change of the incidence angle can be identified through the location of stagnation point near the leading edge on the blade surface. From Fig. 15, it can be seen that the stagnation point (low Mach number location near the leading edge) has been moved from the pressure surface to the nose of the blade, which means the reduction of the incidence angle.

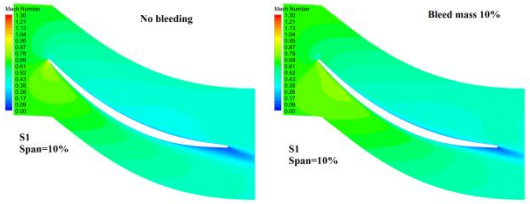

Figure 14 –Contour of relative Mach number on the blade-to-blade surface on 10% span.

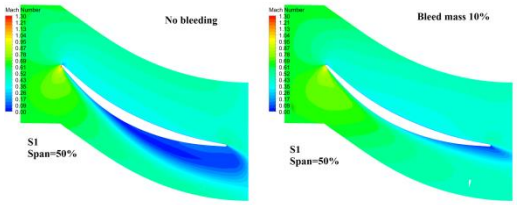

Figure 15 –Contour of relative Mach number on the blade-to-blade surface on 50% span.

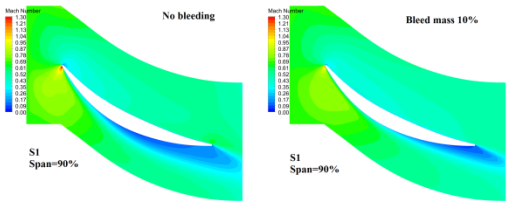

Figure 16 –Contour of relative Mach number on the blade-to-blade surface on 90% span.

The three-dimensional (3D) streamline origin from the circumferential bleed slot via the annular plenum chamber and bleed off through one of the off-take ducts is given in Fig. 17. The contour of Mach number at the off-take duct with bleeding is also shown in Fig. 17. From the comparison of the 3D streamline the circumferential non-uniformity on the circumferential bleed slot is evident by non-axisymmetric bleed (i.e. one duct bleeding). This circumferential non-uniformity bleed through the bleed slot may introduce a total pressure distortion on the stages at the rear part of the bleed slot. This may have effects on the stability of the compressor. This kind of influence is still unknown and need further investigations, however this part is no the topic in this paper and will be

considered in the future studies.

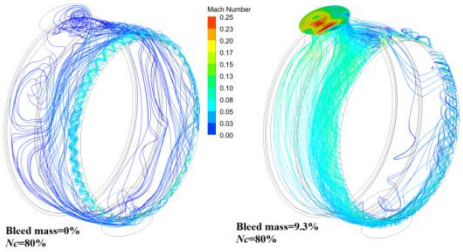

Figure 17 –3D streamline in the bleed system.

5. Conclusions

In this paper, the effect of inter-stage bleeding on flow stability of a multi-stage axial compressor has been investigated through steady numerical calculations. Several conclusions have been drawn from this paper:

(1) The surge margin of the multi-stage axial compressor has been increased through inter-stage bleeding at part speed.

(2) There is an optimal bleed mass flow rate at a specific corrected speed in order to get a maximum surge margin.

(3) The optimal bleed mass flow at different corrected speed changes with the corrected speed; the lower the speed the higher the bleed mass flow rate is needed.

(4) The mechanism of surge margin increase with inter-stage bleed is related to the decrease of the incidence angle of the S1, and the relieved of the blockage at the back-stages. The mismatching of the stages has been relieved.

References

[1] Cumpsty N A. (2004). Compressor Aerodynamics. Reprint Edition. Malabar, Florida: Krieger Publishing Company.

[2] Dixon S. L., and C. A. Hall. (2010). Fluid Mechanics and Thermodynamics of Turbomachinery. Sixth edition, Butterworth–Heinemann, USA.

[3] Leishman, B. A., Cumpsty, N. A., and Denton, J. D., (2007). Effects of Bleed Rate and Endwall Location on the Aerodynamic Behavior of a Circular Hole Bleed Off-Take. ASME J. Turbomach., 129(4): 645–658.

[4] Leishman, B. A., Cumpsty, N. A., and Denton, J. D., (2007). Effects of Inlet Ramp Surfaces on the Aerodynamic Behavior of Bleed Hole and Bleed Slot Off-Take Configurations. ASME J. Turbomach., 129(4): 659–668.

[5] Conan, F., and Savarese, S., (2001). Bleed Airflow CFD Modelling in Aerodynamics Simulations of Jet Engine Compressors. ASME Paper No. 2001-GT-0544.

[6] Wellborn, S. R., and Koiro, M., (2002). Bleed Flow Interactions with an Axial Flow Compressor Powerstream. AIAA Paper No. 2002-4057.

[7] Gomes, R., Schwarz, C., and Peitzner, M., (2005). Aerodynamic Investigations of a Compressor Bleed Air Configuration Typical for Aeroengines. 17th International Symposium on Air Breathing Engines, Munich, Sept. 4–9, Paper No. ISABE-2005-1264.

[8] Gomes, R., and Schwarz, C., (2006). Experimental Investigation of a Generic Compressor Bleed System. ASME Paper No. GT2006-90458.

Copyright Statement